A New Damage Mechanics Based Approach for Integrity Assessment of Plant Components

M. K. Samal[1]

Abstract: Safety analysis of critical components and the overall plant is a major and important task in the field of mechanical engineering. Therefore, it is essential to know the allowable loads and the corresponding failure behaviour (e.g., crack initiation, growth and instability) of the component. The damage mechanics approaches which incorporate the microscopic processes of ductile fracture (i.e., void nucleation, growth and coalescence) into the material constitutive behaviour has been very successful in predicting the ductile crack propagation in specimens and components irrespective of their geometry, loading types etc. The major drawback of these models is the requirement of a pre-defined size of discretization for the numerical treatment. Hence, these models are not capable of simulation of fracture behaviour in several situations such as miniature specimens, thin films, ductile-to-brittle transition regime (where the stable crack growth is of the order of few microns before cleavage initiation), bi-material interface (requirement of different discretization sizes across the interface), zones with steep stress gradients etc. In this work, a new damage mechanics approach based on a nonlocal regularization scheme has been developed and its advantages in tackling the above-mentioned problems has been demonstrated through various examples.

Keywords: Nonlocal model; Damage mechanics; Rousselier's model; Finite element implementation; Ductile-to-brittle transition; Fracture toughness master curve

1   Introduction

Prevention of failure of pressurized and high-energy components and systems has been an important issue in the design of all types of power and process plants. Instead of the traditional fracture mechanics based approaches, it is now possi-

---

[1] Reactor Safety Division, Bhabha Atomic Research Centre, Trombay, Mumbai. E-mail: mk-samal@barc.gov.in. Current address: Department of Mechanical Engineering, Ohio State University, Columbus, Ohio. E-mail: samal.3@osu.edu, Tel: +1-614-6883288

ble to go for the detailed modeling of different fracture or material degradation processes using local approaches [Rice and Tracey (1969); Rousselier (1987); Gurson (1977)]. There are two classes of local approaches, i.e., uncoupled and coupled types. In the uncoupled type of models (e.g., Rice and Tracey's model [Rice and Tracey (1969)]), the material damage is evaluated from the local stress and strain fields in a post-processing exercise. In the coupled type of models (popularly known as continuum damage models), the effect of material damage is usually considered as an internal variable in the expressions representing the constitutive behaviour of engineering materials (e.g., Rousselier's [Rousselier (1987)] and Gurson-Tvergaard-Needleman's [Gurson (1977); Tvergaard and Needleman (1984); Needleman and Tvergaard (1984)] model). These local damage models have been used by many researchers to predict the load-deformation and fracture resistance behaviour of different types of specimens and components [Kussmaul, Eisele and Seidenfuss (1995); Pitard-Bouet, Seidenfuss, Bethmont and Kussmaul (1999); Pavankumar, Samal, Chattopadhyay, Dutta, Kushwaha, Roos and Seidenfuss (2005); Eberle, Klingbeil and Schicker (2000)]. Numerical analyses based on these local damage models, however, are often found to depend on the spatial discretization (i.e., mesh size of the numerical method used). The increasingly finer discretization grids can lead to earlier crack initiation and faster crack growth [Bazant and Belytschko (1987); Aifantis (2001); Geers, de Borst, Brekelmans and Peerlings (1998); Peerlings, De Borst, Brekelmans, and Geers (2002); Reusch, Svendsen and Klingbeil (2003); Reusch, Svendsen and Klingbeil (2003); Svendsen (1999); Samal, Seidenfuss, Roos, Dutta and Kushwaha (2008); Samal, Seidenfuß Roos, Dutta, Kushwaha (2007); Rettenmeier (2009); Roos, Schuler, Silcher, Seebich and Eisele (2005); Seidenfuss and Roos (2004)]. The major drawback of these models is the requirement of a pre-defined size of discretization for the numerical treatment. Hence, these models are not capable of simulation of fracture behaviour in several situations such as miniature specimens, thin films, ductile-to-brittle transition regime (where the stable crack growth is of the order of few microns before cleavage initiation), bi-material interface (requirement of different discretization sizes across the interface), zones with steep stress gradients etc.

In this paper, the author has regularized the Rousselier's model with the help of a nonlocal damage parameter, the evolution of which is related to the local void volume fraction through a diffusion type equation. This damage diffusion equation has been discretized alongwith the stress equilibrium equation using finite element method. In order to predict the cleavage fracture probability in the DBT region, Beremin's model for cleavage fracture [Beremin (1983)] needs to be coupled with the continuum damage mechanics model for ductile fracture. When simulating the crack tip stress field at a lower temperature (when stress gradients are large) us-

ing finite element (FE) method, one needs to use a very fine discretization, which cannot be used for the classical (or local) damage mechanics model as the discretization size is pre-defined for a material (which is typically of the order of 0.2mm). This order of FE discretization is too coarse to accurately capture the low temperature crack tip stress field and hence the Weibull parameters are unable to predict the fracture toughness transition curve when the classical damage mechanics or elasto-plastic models are combined with the Beremin's model. Many times, an empirical variation of Weibull parameters with temperature has been suggested in literature [Seebich (2007); Gao, Ruriggieri and Dodds (1998); Gao, Dodds, Tregoning, Joyce and Link (1999); Gao, Dodds, Tregoning and Joyce (2001); Gao and Dodds (2005); Petti and Dodds (2005)] for prediction of the fracture toughness transition curve [Wallin, K. (1991); Wallin, K. (1991); ASTM-E 1921-05 (2005); Eisele (2006)] along with the use of elasto-plastic analysis for calculation of Weibull stress. However, the problem lies in the inability to model small amounts of ductile crack growth (before unstable cleavage fracture) in the FE analysis. Again, the minimum amount of stable crack growth that can be simulated is of the order of one element size. In the experiments, it is usually observed that the average stable crack growth (before instability) is of the order of 0.2 mm at -20 deg. C and hence to simulate very small amounts of crack growth (of the order of one-tenth of 0.2 mm), one requires mesh sizes of the order of 0.02 mm. It is now clear that the local damage models cannot be used for these mesh sizes and hence the use of nonlocal formulation has been investigated in this work. The paper is organised in seven sections. The ability of local damage models to simulate structural response for various geometry and loading conditions have been demonstrated in Section-2. The disadvantages of these models to predict the response in several other situations have been outlined in Section-3. The concept of nonlocal regularization scheme adopted in this work is described in Section-4 followed by an outline of its numerical implementation in a finite element framework in Section-5. Several examples have been presented in Section-6 to demonstrate the advantages of the new nonlocal formulation over the local one followed by conclusions and scope of future research in Section-7.

2   Local damage model and simulation of structural response for various geometry and loading conditions

The microscopic processes of ductile fracture involve the stages such as void nucleation, growth and coalescence. This can be observed experimentally by preparing specimens for observation in scanning electron microscope (SEM) from the regions near to the crack tip in case of a fracture mechanics specimen or near to the region of cup-cone fracture in case of a tensile specimen. An axi-symmetric

round tensile specimen from the material SA333 Gr.6 (which is used as primary heat transport piping material of Indian pressurized heavy water reactors) was prepared and loaded in tension till fracture. Small discs were machined from regions near to the fracture surface and these were suitably polished for SEM observation. The distinct process of nucleation of voids (around inclusions and second phase particles) in this material can be observed from Fig. 1(a). The voids start growing under the influence of plastic strain and hydrostatic stress as shown in Fig. 1(b) and the voids coalescence by rupture of adjoining ligaments as seen in Fig. 1(c).

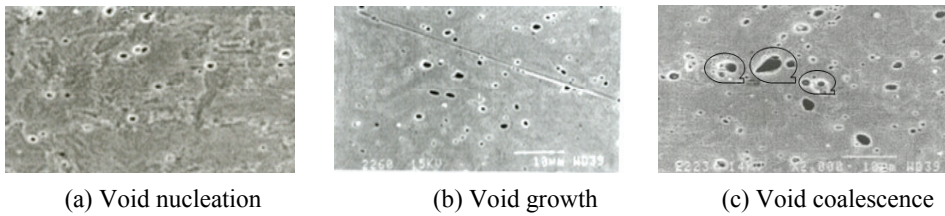(a) Void nucleation   (b) Void growth   (c) Void coalescence

Figure 1: Scanning electron microscope images of the microscopic stages of ductile fracture process as observed in a low alloy steel (SA333 Gr.6 carbon steel)

Though cumbersome, these SEM images can be even used to quantify the void fractions and their evolution with loading. A combination of suitable FE analysis and SEM data can provide estimates of the micro-mechanical parameters used in the damage models (as discussed in the following paragraphs). In order to incorporate these microscopic stages of ductile fracture in the material constitutive models, a representative volume element is developed as demonstrated in Fig. 2. This RVE is the gateway for the bridging the length-scale from the microscopic scale to the continuum scale. This is done through an internal state variable 'f' which is denoted as the ductile void volume fraction (as this represents the volume of the void to the volume of the unit cell). The state variable 'f' is incorporated into the material yield criterion (e.g., in case of Rousselier model) as

$$\varphi = \frac{\sigma_{eq}}{1-f} + D\sigma_k f \exp\left(\frac{-p}{(1-f)\,\sigma_k}\right) - R(\varepsilon_{eq}) = 0 \qquad (1)$$

where σ_{eq} is the von-Mises equivalent stress, D and σ_k are the material constants, p is the mean hydrostatic pressure and $R(\varepsilon_{eq})$ is the material resistance (i.e., stress-strain curve), which is a function of equivalent plastic strain ε_{eq}. This yield criterion of Eq. (1) falls into the class of porous metal plasticity criteria.

The essence of this model is that it reduces to the classical von-Mises criterion when the void volume fraction 'f' is zero (i.e., a perfect continuum). On the other
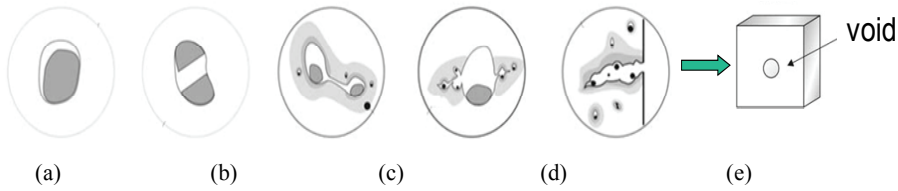
Figure 2: Schematic representation of the processes voids nucleation, growth and coalescence and its incorporation into the representative volume element (RVE) as an internal state variable. (a) Debonding of the particle from matrix nucleating a void, (b) Cracking of a particle nucleating a void, (c) Ligament rupture between two particle in the shear-band causing void coalescence, (d) Interaction of smaller voids with a dominant void, (e) Stable crack growth in the ductile matrix, (f) Representation of the damage in (e) with an equivalent continuum RVE with void volume fraction 'f' as an internal state variable

hand, the yield surface shrinks to a point when the void volume fraction 'f' becomes unity representing the complete loss of material stiffness as there is no material in the RVE. The other essence of this model is that the yielding of the material also becomes dependent upon the state of hydrostatic stress because of the presence of voids and the material stress carrying capability reduces exponentially with increase in void volume fraction 'f' and positive hydrostatic stress. In reality, the stress carrying capability of the RVE falls drastically after the void volume fraction exceeds a critical value 'f_c', called the critical void volume fraction representing the void coalescence. The micro-mechanical parameters required for the analysis are: (a) initial void volume fraction 'f_0', (b) critical void volume fraction for coalescence 'f_c', (c) final void volume fraction for fracture 'f_f', (d) void volume fraction at saturated condition of nucleation 'f_n', (e) mean strain for void nucleation 'ε_n', (f) standard deviation for void nucleation strain 's_n', (g) magnitude of numerical discretization (l_c). As discussed earlier, these can be determined from a combined metallographic study and FE analysis. The details can be found in Ref. [Pavankumar, Samal, Chattopadhyay, Dutta, Kushwaha, Roos and Seidenfuss (2005)].

The advantage of these models is that the process of crack initiation and growth are implicit in the formulation as the damage is coupled to the state of stress. There is no need to assume an initial crack to start the analysis (which is the requirement when the fracture mechanics methods are applied to carry out structural safety analysis). Moreover, the micro-mechanical parameters are dependent only upon the material and hence, these are transferable across different geometry and loading conditions unlike the fracture mechanics parameters such as J_{IC} and J-R curves. In
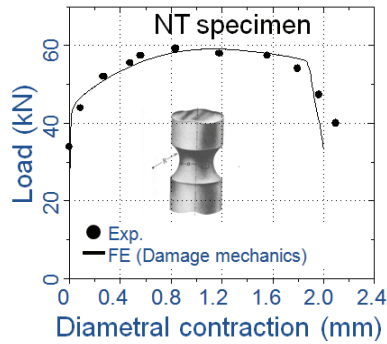
Figure 3: Comparison of response predicted for a notched tensile (NT) specimen with experiment
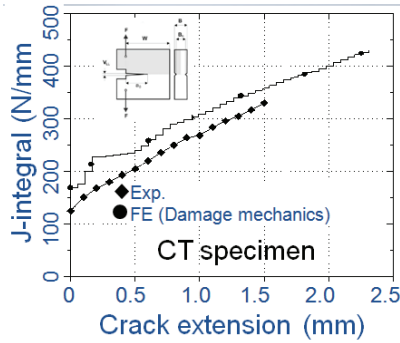

Figure 4: Comparison of response predicted for a compact tension (CT) specimen with experiment

order to demonstrate the points discussed in this section, let us look at the results from simulations from such a model using the Rousselier's yield criterion as specified in Eq. (1). In Fig. 3, an axi-symmetric notched tensile specimen of material Ste460 is loaded in tension and the load-diametral contraction response is recorded. The local damage model is used to predict the response of the specimen and this is compared in Fig. 3. It can be observed that the damage model is able to predict the point of load drop (due to initiation of cup-cone fracture) very accurately. The model is subsequently used to predict the fracture resistance behaviour of a standard compact tension (CT) specimen from the same material. As the material remains same, the same micro-mechanical parameters have been used in the simulation and the predicted fracture resistance (J-R) curve has been compared with that

of experiment in Fig. 4. The correspondence between experimental and simulated J-R curves is very good. In order to demonstrate the ability of the damage mechanics models to predict the response of actual plant components such as straight pipes and pipe bends, simulations are also carried out in 3D domain with different loading configurations as shown in Fig. 5 and 6 respectively. In Fig. 5, a straight pipe with 8-inch nominal diameter with a 120 degree through-wall circumferential crack is loaded in four-point bending. These pipes are common in the primary heat transfer circuit of Indian pressurized heavy water reactors. The material is a low alloy carbon steel SA333Gr.6. In Fig. 6, a 90° bent pipe (elbow) made of the same material and of same 8-inch nominal bore with circumferential through-wall crack at the extra-dos location is loaded with closing end-moments. The predicted load-displacement curves for both the components are compared with those of experiment and the results of elasto-plastic analysis (without damage in the material constitutive equations). The elasto-plastic material model is not able to consider the effect of stiffness degradation due to crack growth and hence, the predicted loads are higher for all the applied displacements. However, the predictions of damage mechanics model are very close to those of experiments. Hence, these models can be safely used for a realistic safety analysis.
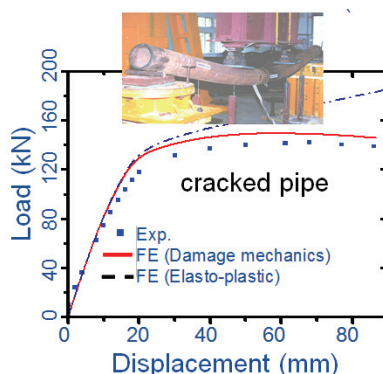

Figure 5: Comparison of response predicted for a straight pipe with circumferential through-wall crack (loaded in four point bending) with experiment

3   Limitations of local damage models

It has been mentioned in the previous section that the local damage models can predict the response during crack growth accurately with a set of micro-mechanical parameters. However, we also need to restrict the smallest size of numerical discretization to a particular value, i.e. 'l_c'. This discretization size is of the order of
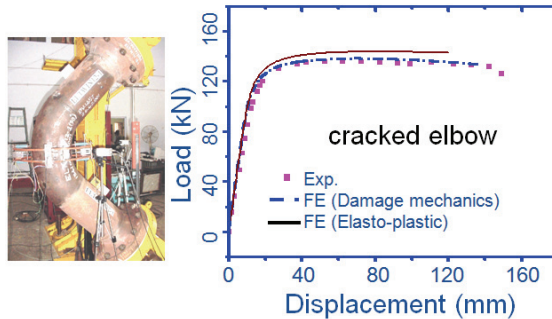
Figure 6: Comparison of response predicted for a 90° bent pipe (elbow) with circumferential through-wall crack at the extra-dos location (loaded with closing end-moments) with experiment

0.2 to 0.4 mm for typical pressure vessel and piping materials as used in nuclear and thermal power plants. However, this poses a limitation from the point of mesh refinement in order to obtain better and converged results in many cases involving steep stress gradients. Many other situations can also be cited where such a requirement is inadequate for the analysis such as, simulation of miniature specimens, thin films, simulation of fracture resistance behaviour in the ductile-to-brittle transition regimes (where the stable crack growth is of the order of few microns before cleavage initiation), and simulation of crack growth in the bi-material interface (requirement of different discretization sizes across the interface due to the existence of different material properties) etc.

The inability of the local damage models is emphasized here with some examples. Fig. 7 shows the load-CMOD (crack mouth opening displacement) response of a standard 1T compact tension (CT) specimen as predicted by the local damage model when three different sizes of FE mesh are used in the crack propagation region (i.e., 0.4, 0.2 and 0.1 mms respectively). The actual experimentally obtained response is also shown in Fig. 7 for comparison. It is obvious that the predictions of the local damage model show pathological mesh size dependence. Another example of such a limitation of the local damage model is shown in Fig. 8. In this figure, the fracture toughness as obtained from experiment using standard 1T CT specimens tested at various sub-zero temperatures are plotted as a function of temperature. One can see a considerable scatter in the data over the whole temperature range of the ductile-to-brittle transition (DBTT) region. Both the mean value and scatter of the fracture toughness data increases with increase in temperature.

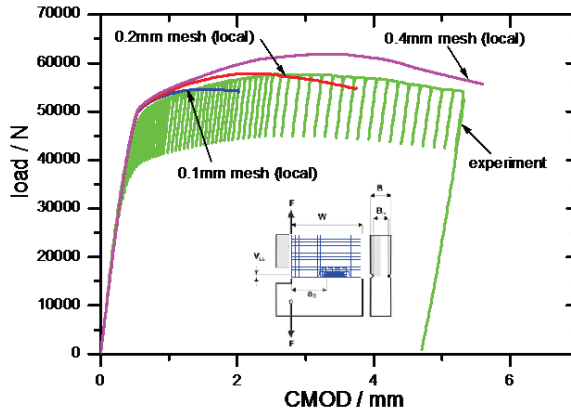This is due to the existence of two competing mechanisms, i.e., unstable cleavage

Figure 7: Predicted load-CMOD response of a compact tension specimen with a local damage model with different FE mesh sizes

fracture and stable crack growth in the DBTT regime. Moreover, the stable crack growth (before failure by unstable cleavage) is of the order of 200 microns only at -20 deg. C, whereas this of the order of few microns at -60 deg. C and below (Fig. 8). The local damage models cannot be applied to simulate the crack growth of the above-mentioned magnitudes as the minimum mesh size (i.e., the dimension of a single element) is above this range. Elasto-plastic analysis cannot predict the stress and strain field correctly due to the non-consideration of damage evolution. In order to elaborate this point, results have been obtained from analysis of the 1T CT specimens with local damage models at various temperatures in the transition regime and these have been compared with the experimental data in Fig. 8. As can be seen from the data, the results of simulation are much off from the experimental mean and scatter values. Hence, this motivates the consideration of a mesh-independent damage model for structural safety analysis.

4 Concept of nonlocal regularization

As discussed in the previous section, the results of analysis using a local damage model are dependent on the size of discretization used in the numerical treatment. Due to the onset of damage, material softening takes place and this changes the nature of the governing differential equation (e.g., loss of ellipticity for elasto-static problems and loss of hyperbolicity for elasto-dynamic problems [Peerlings, De Borst, Brekelmans, and Geers (2002)]). When the microscopic aspect of material damage is considered, it can be realized that damage development in a microstructure is not strictly a point-function. It depends upon the state of stress, strain
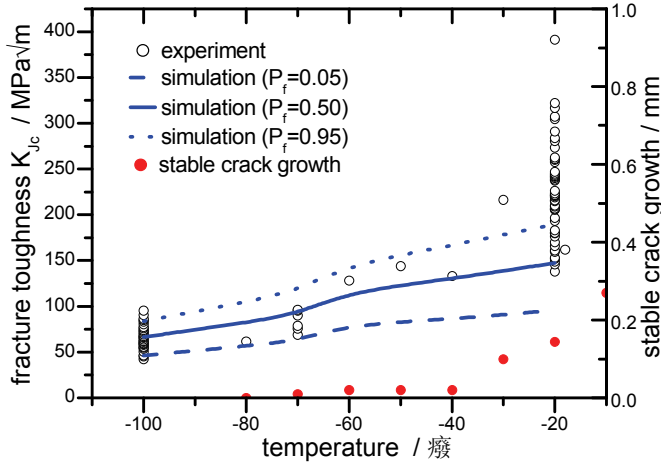
Figure 8: Inability of elasto-plastic and local damage models to predict fracture toughness transition curve in the DBTT regime

and damage of the surrounding regions also due to the underlying micro-structure (i.e., grain boundary, dislocations, dislocation sources and obstacles etc.). More-over, there are phenomena involving motion of dislocations which drive the plastic deformation and damage accumulation due to dislocation pile-up at the obstacles etc. which are not explicitly represented in continuum mechanics formulations. Hence, we need a regularization technique where the damage development in a material point will be coupled to the state of damage of surrounding points in a region with a characteristic dimension, which depends upon the material.

Such a scheme is outlined in Fig. 9. Figure 9 shows the importance of consideration of influence of surrounding points on the damage development at a material point. The weight given to the points nearer to the point under consideration should higher and it diminishes exponential with distance from the above point. Such a weightage scheme is shown in Fig. 9 which is the Gaussian weight function Ψ. The increment of the nonlocal variable in a material point $\vec{x}$, i.e. the increment of nonlocal void volume fraction $\dot{d}$, is mathematically defined as a weighted average of the increment of the local void volume fraction $\dot{f}$ in a domain Ω [Fig. 9], i.e.,

$$\dot{d}(\vec{x}) = \frac{1}{\Psi(\vec{x})} \int\limits_{\Omega} \Psi(\vec{y};\vec{x})\dot{f}(\vec{y}) \, d\Omega(\vec{y}) \tag{2}$$

where $\vec{y}$ is the position vector of the infinitesimally small volume $d\Omega$. In this work, the nonlocal treatment is performed on the damage rate and not on the damage. This
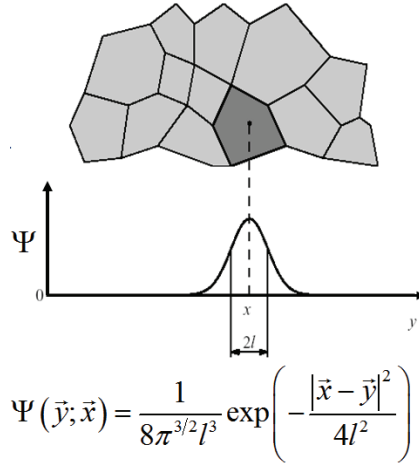
$$\Psi\left(\vec{y};\vec{x}\right) = \frac{1}{8\pi^{3/2}l^3}\exp\left(-\frac{|\vec{x}-\vec{y}|^2}{4l^2}\right)$$

Figure 9: Definition of the nonlocal variable an integral of local void volume fraction 'f' over the shaded characteristic region with a Gaussian function as weight

has been done in order to make it convenient for use in the subsequent incremental nonlinear FE formulation of the problem. The function $\Psi\left(\vec{y};\vec{x}\right)$ is the Gaussian weight function given by

$$\Psi\left(\vec{y};\vec{x}\right) = \frac{1}{8\pi^{3/2}l^3}\exp\left(-\frac{|\vec{x}-\vec{y}|^2}{4l^2}\right) \tag{3}$$

and the normalisation factor is the integral of the Gaussian weight function, i.e.,

$$\Psi\left(\vec{x}\right) = \int_{\Omega}\Psi\left(\vec{y};\vec{x}\right)d\Omega \tag{4}$$

The length parameter l determines the size of the volume, which effectively contributes to the nonlocal quantity and is related to the scale of the microstructure. The above integral nonlocal kernel holds the property that the local continuum is retrieved if $l \rightarrow 0$. By expanding $\dot{f}\left(\vec{y}\right)$ in Taylor's series around the point x, we get

$$
\begin{aligned}
\dot{f}\left(\vec{y}\right) = {}& \dot{f}\left(\vec{x}\right) + \frac{\partial \dot{f}}{\partial x_i}\left(y_i - x_i\right) + \frac{1}{2!}\frac{\partial^2 \dot{f}}{\partial x_i \partial x_j}\left(y_i - x_i\right)\left(y_j - x_j\right) \\
& + \frac{1}{3!}\frac{\partial^3 \dot{f}}{\partial x_i \partial x_j \partial x_k}\left(y_i - x_i\right)\left(y_j - x_j\right)\left(y_k - x_k\right) \\
& + \frac{1}{4!}\frac{\partial^4 \dot{f}}{\partial x_i \partial x_j \partial x_k \partial x_l}\left(y_i - x_i\right)\left(y_j - x_j\right)\left(y_k - x_k\right)\left(y_l - x_l\right) + \dots
\end{aligned}
\tag{5}
$$

where Einstein's summation convention applies to the indices i, j, k and l. Substituting Eq. (5) into Eq. (2), we get

$$\dot{d}(\vec{x}) = \dot{f}(\vec{x}) + C_{length}\nabla^2\dot{f}(\vec{x}) + d_{length}\nabla^4\dot{f}(\vec{x}) + ... \tag{6}$$

where the Laplacian operator is defined by $\nabla^2 = \sum_i \frac{\partial^2}{\partial x_i^2}$ and $\nabla^4 = (\nabla^2)^2$ etc. The gradient parameters C_{length} and d_{length} have the dimensions of length to an even power and the odd derivatives of Eq. (5) vanish due to the nature of the Gaussian weight function of Eq. (3) when substituted in Eq. (2). Taking the Laplacian of Eq. (6), we obtain

$$\nabla^2\dot{d}(\vec{x}) = \nabla^2\dot{f}(\vec{x}) + C_{length}\nabla^4\dot{f}(\vec{x}) + d_{length}\nabla^6\dot{f}(\vec{x}) + ... \tag{7}$$

Substracting C_{length}x Eq. (6) from Eq. (7), we obtain Eq. (8) when the terms containing $\nabla^4\dot{f}(\vec{x})$ and other higher order terms are neglected.

$$\dot{d} - \dot{f} - C_{length}\nabla^2\dot{d} = 0 \tag{8}$$

The above Eq. (8) is the diffusion equation for damage and the increment of the nonlocal variable 'd' is linked to the increment of local void volume fraction 'f' though a characteristic length parameter 'C_{length}' and the Laplacian of increment of nonlocal damage 'd'. This is an implicit description of damage diffusion and it needs to be solved along with the mechanical equilibrium equation as discussed in the following section.

5   Numerical implementation in a finite element framework

For numerical simulations, a nonlocal form of the material yield surface has been constructed from the classical Rousselier's model [2] as shown in Eq. (9) below. In this yield function, the void volume 'f' is replaced by the nonlocal material damage 'd' as

$$\varphi = \frac{\sigma_{eq}}{1-d} + D\sigma_k d\exp\left(\frac{-p}{(1-d)\sigma_k}\right) - R(\varepsilon_{eq}) = 0 \tag{9}$$

The equilibrium equation in the continuum to be solved along with the damage diffusion equation (8) is written as

$$\nabla.\sigma + f_b = 0 \tag{10}$$

The associated boundary conditions are

$$\sigma.n|_{\Gamma_f} = f_m \tag{11}$$

$$u|_{\Gamma_u} = u_0 \tag{12}$$

$$\nabla \dot{d}.n|_{\Gamma_d} = 0 \tag{13}$$

where σ_{ij} is the Cauchy stress tensor and f_b is the body force per unit volume and f_m is the applied mechanical traction at the surface. Eq. (11) is the traction or force boundary condition, $n|_{\Gamma_f}$ is the normal to the boundary Γ_f, Eq. (12) is the geometric or essential displacement boundary condition and Eq. (13) is the Neumann or force boundary condition for the damage degree of freedom and $n|_{\Gamma_d}$ is the normal to the boundary Γ_d of the domain $\Omega_{t+\Delta t}$. In our analysis, we employ an incremental procedure and use the updated Lagrangian formulation to express the equilibrium configuration of the body. Assuming additive decomposition of total strain increment into elastic $\dot{\varepsilon}^e$ and plastic $\dot{\varepsilon}^p$ parts, we can write

$$\dot{\varepsilon} = \dot{\varepsilon}^e + \dot{\varepsilon}^p \tag{14}$$

The yield function can be written in terms of mean hydrostatic and deviatoric parts of stress tensor and other field variables as

$$\varphi(p,q,H^\alpha,d) = 0 \tag{15}$$

where p and q are the hydrostatic pressure and von Mises equivalent stress respectively and are defined as

$$p = -\tfrac{1}{3}\sigma : I$$
$$q = \left(\tfrac{3}{2}s : s\right)^{1/2} \tag{16}$$

H^α is internal state variable such as hardening, I is the kronecker-delta or second order indentity tensor, s is the deviatoric part of stress tensor σ. The increase in void volume fraction (due to combined void nucleation and growth process) during plastic deformation in the ductile fracture process can be written as a function F, i.e.,

$$F(p,q,H^\alpha,d) = \dot{f} = \dot{f}_{growth} + \dot{f}_{nucleation} = (1-d)\dot{\varepsilon}^p : I + A(\varepsilon_{eq})\dot{\varepsilon}_{eq} \tag{17}$$

where $\dot{\varepsilon}^p$ is the increment in plastic strain tensor ε^p, I is the tensor equivalent to Kronecker-Delta function, $\dot{\varepsilon}_{eq}$ is the increment in equivalent plastic strain of the matrix material and A is the void nucleation constant which obeys Gaussian distribution (as a function of ε_{eq}) and can be expressed as

$$A(\varepsilon_{eq}) = \frac{f_N}{s_N\sqrt{2\pi}} \exp\left(-\frac{1}{2}\left(\frac{\varepsilon_{eq} - \varepsilon_N}{s_N}\right)^2\right) \tag{18}$$

The constitutive behaviour of the new material model can be finally obtained in the following forms (i.e., increment of stress tensor and increment of void fraction potential) as functions of increment of total strain tensor and damage variable

$$\partial \sigma = \underline{\underline{C_{ep}}} : \partial \varepsilon + \underline{C_{ed}} : \partial d \tag{19}$$

and

$$\partial F = \underline{C_{de}} : \partial \varepsilon + C_{dd} : \partial d \tag{20}$$

where the material tangent stiffness matrices can be defined as

$$
\begin{aligned}
\underline{\underline{C_{ep}}} &= 2G\frac{q}{q^{tr}}J' + K\left(1 - m_{pl}\right)II + \frac{4}{3}G\left(1 - \frac{q}{q^{tr}} - \frac{3}{2}m_{qn}\right)nn - 2Gm_{ql}nI - Km_{pn}In \\
\underline{C_{ed}} &= -2Gm_{qd}n - Km_{pd}I \\
\underline{C_{de}} &= C_{d11}\left(m_{pl}I + m_{pn}n\right) + C_{d12}\left(m_{ql}I + m_{qn}n\right) + C_{d13}n + C_{d14}I \\
C_{dd} &= C_{d11}m_{pd} + C_{d12}m_{qd} + C_{d15}
\end{aligned}
\tag{21}
$$

In the above expression, J is the fourth order unit tensor and $J' = J - \frac{II}{3}$. The details of the derivation and the co-efficients of Eq. (21) can be found in Ref. [Samal, Seidenfuss, Roos, Dutta and Kushwaha (2008)]. For implementation of the above model in a finite element framework, the weak forms of the governing equations are expressed in the updated Lagrangian setting as

$$
{}^{t+\Delta t}R = \int_{{}^{t+\Delta t}\Omega} {}^{t+\Delta t}f_{b_i}\delta u_i d^{t+\Delta t}\Omega + \int_{{}^{t+\Delta t}\Gamma_f} {}^{t+\Delta t}t_{s_i}\delta u_i d^{t+\Delta t}\Gamma_f \tag{22}
$$

and

$$
\int_{\Omega} \delta \dot{d} \left(\dot{d} - \dot{f} - C_{length}\nabla^2 d\right).d\Omega = 0 \tag{23}
$$

respectively. Expressing the generalised displacement, strain and damage vectors at any material point inside the finite element in terms of the generalized nodal variables ($\hat{u}$ and $\hat{d}$) as [Fig. 10]

$$
\begin{aligned}
u &= N_u\hat{u}, \quad {}_{t+\Delta t}e = B_u\hat{u} \\
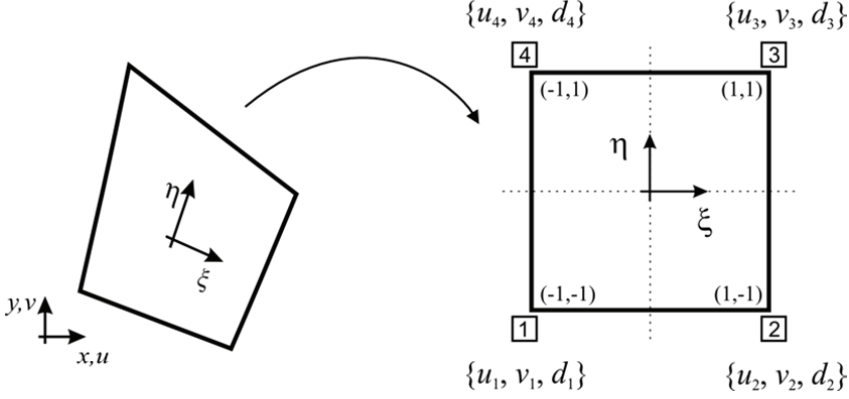\dot{d} &= N_d\hat{d}, \quad \nabla d = B_d\hat{d}
\end{aligned}
\tag{24}
$$

Figure 10: An arbitrary region mapped into 4-noded master element with damage as an extra nodal degree of freedom

where N_u and N_d are the shape function matrices for the displacement and nonlocal damage variable, B_u and B_d are matrices containing the derivatives of the shape function N_u and N_d respectively. Expanding Eqs. (22) and (23), using consistent material matrices from Eqs. (21) and substituting the expressions for $u_{,t+\Delta t}e, d$ and ∇d from Eqs. (24), we get the following equations

$$\delta\left(\Delta\hat{u}\right)^T$$

$$
\begin{bmatrix}
\left(\int_{\Omega} B_u^T \underline{\underline{C_{ep}}} B_u.d\Omega\right)\Delta\hat{u} + \left(\int_{\Omega} B_{NL}^T {}^{t+\Delta t}\underline{\underline{\sigma}} B_{NL}.d\Omega\right)\Delta\hat{u} + \left(\int_{\Omega} B_u^{T\,t+\Delta t}\sigma B_{NL}.d\Omega\right) \\
+ \left(\int_{\Omega} B_u^T \underline{\underline{C_{ed}}} N_d.d\Omega\right)\hat{d} - \int_{\Omega} N_u^T f_b d\Omega - \int_{\Gamma} N_u^T t_s d\Gamma
\end{bmatrix}
$$

$$= 0 \quad (25)$$

$$
\delta\hat{d}^T
\begin{bmatrix}
\left(\int_{\Omega} N_d^T N_d.d\Omega\right)\hat{d} - \left(\int_{\Omega} N_d^T \underline{\underline{C_{de}}} B_u.d\Omega\right)\hat{u} \\
- \left(\int_{\Omega} N_d^T C_{dd} N_d.d\Omega\right)\hat{d} + \left(\int_{\Omega} B_d^T C_{length} B_d.d\Omega\right)\hat{d} \\
+ \int_{\Omega} N_d^{T\,t+\Delta t}d\; d\Omega - \int_{\Omega} N_d^{T\,t+\Delta t}\hat{f}\; d\Omega + \int_{\Omega} B_d^T C_{length}{}^{t+\Delta t}\nabla d\; d\Omega
\end{bmatrix}
= 0 \quad (26)
$$

where t_s is the surface traction and is given as $t_s = \sigma. n|_{\Gamma_f}$ (Cauchy's traction law), ${}^{t+\Delta t}\underline{\underline{\sigma}}$ is the matrix and ${}^{t+\Delta t}\sigma$ is the vector containing Cauchy's stress components at time $t + \Delta t$ and B_{NL} is the nonlinear strain-displacement transformation matrix. For arbitrary value of $\delta\left(\Delta\hat{u}\right)^T$ and $\delta\hat{d}^T$, the terms inside the brackets of Eqs. (25)

and (26) should be zero and hence these equations reduce to the set of finite element algebraic equations, which can be written in convenient (matrix) form as

$$A\left(\begin{bmatrix} K_{uu}+K_{NL} & K_{ud} \\ K_{du} & K_{dd} \end{bmatrix} \begin{Bmatrix} \Delta\hat{u} \\ \Delta\hat{d} \end{Bmatrix}\right) = A\left(\begin{Bmatrix} f_m^{ext}-f_m^{int} \\ -f_d^{int} \end{Bmatrix}\right) \tag{27}$$

where A is the assembly operator which is used to assemble to element stiffness matrices and the matrices and force vectors of all the elements in the domain Ω. The domain and boundary of each element are represented by Ω^e and Γ^e respectively. Hence the element level stiffness and force vectors can be written as

$$\begin{aligned}
K_{uu} &= \int_{\Omega^e} B_u^T \underline{\underline{C_{ep}}} B_u.d\Omega \\
K_{NL} &= \int_{\Omega^e} B_{NL}^{T} \underline{\underline{^{t+\Delta t}\sigma}} B_{NL}.d\Omega \\
K_{ud} &= \int_{\Omega^e} B_u^T \underline{C_{ed}} N_d.d\Omega \\
K_{du} &= - \int_{\Omega^e} N_d^T \underline{C_{de}} B_u.d\Omega \\
K_{dd} &= \int_{\Omega^e} N_d^T N_d.d\Omega - \int_{\Omega^e} N_d^T C_{dd} N_d.d\Omega + \int_{\Omega^e} B_d^T C_{length} B_d.d\Omega \\
f_m^{ext} &= \int_{\Omega^e} N_u^T f_b d\Omega + \int_{\Gamma^e} N_u^T t_s d\Gamma \\
f_m^{int} &= \int_{\Omega^e} B_u^{T^{t+\Delta t}}\sigma.d\Omega \\
f_d^{int} &= \int_{\Omega^e} N_d^{T^{t+\Delta t}}d.d\Omega - \int_{\Omega^e} N_d^{T^{t+\Delta t}}f.d\Omega + \int_{\Omega^e} B_d^T C_{length}\nabla^{t+\Delta t}d.d\Omega
\end{aligned} \tag{28}$$

where the left superscript $'t+\Delta t'$ refers to the quantities at the end of current time step [and the values are at the previous iteration process $(i-1)$] of the incremental nonlinear finite element analysis. When the iteration process converges, the values of the variables at iteration steps i and $(i-1)$ also converge. The assembled global FE equations are solved for the global degrees of freedom when we specify the required boundary and loading conditions. It may be noted that the assembled (i.e., global) internal damaged force vectors of the elements becomes a null vector. The stiffness terms K_{ud}, K_{du} and K_{dd} in the element stiffness matrix are contributions of the new nonlocal formulation.

6   Results and Discussion

In order to demonstrate the efficacy of the nonlocal damage model as discussed in the previous section, we provide several examples in this section and discuss the results. The first example is the demonstration of the mesh-independent nature of the solutions. The standard 1T compact tension specimen is simulated again with the new model with different sizes of discretization in the crack propagation

region. The material of the CT specimen is DIN 22NiMoCr3-7 which is a pressure vessel steel material. The results of the numerical simulation for all the mesh sizes are shown in Fig.11 along with the experimental data. It can be observed that the results of the new model are mesh-independent and they are also very close to the experimental data. There are other advantages of the nonlocal model. One such example is the consideration of symmetric boundary conditions in the analysis. These boundary conditions are widely used by analysts by taking advantage of the different symmetry in the component geometry, loading and boundary conditions in order to reduce the cost and time of computation.
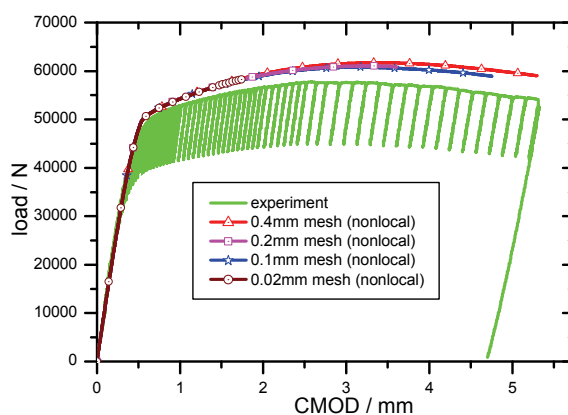
Figure 11: Predicted mesh-independent load-CMOD response of the CT specimen by the nonlocal model

The results of analysis should not be dependent upon such an assumption which is a mathematical representation of the actual physical domain. In the forthcoming discussion, it has been demonstrated that the results of analysis with local damage model violates such as assumption. Fig. 12(a) shows the axi-symmetric FE mesh of a flat plate with a hole at the centre and loaded in tension. The analysis is carried out considering plane strain condition of loading. The FE mesh with symmetric boundary condition at the centre is shown in Fig. 12(b). When the symmetric mesh is used, the crack propagation is restricted to the bottom layer of elements in the FE mesh of Fig. 12(b). As the model is symmetric about the central line passing through the hole, this represents a symmetric crack propagation along two element layers (one at the top half and the other at the bottom half). The same should be predicted if we choose to use the full model without symmetric boundary conditions, i.e., mesh of Fig. 12(a).
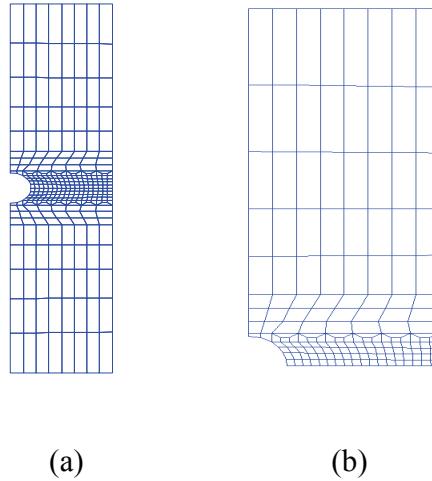
(a)   (b)

Figure 12: (a) FE mesh of half of the flat tensile specimen with hole at the centre, (b) FE mesh with symmetry boundary conditions

However, the results of analysis for the full model with the local formulation are shown in Fig. 13, which clearly shows that the crack path is asymmetric and still along one element layer and hence, it is against our earlier expectation. However, the nonlocal model preserves the symmetric nature of the crack propagation path as this loading is symmetric as can be seen from Fig. 14. Hence, the nonlocal models have a clear advantage over the local formulation. The difference in the nominal stress vs %age hole opening behaviour for both cases is shown in Fig. 15 and the results are same for the nonlocal model for both the cases, whereas it is different for the local model.

The other example is the prediction of load-CMOD response of different sizes of compact tension specimen ranging from 1T (1 inch thickness) to 4T (4 inch thickness). Experimental data are available for the first two sizes, i.e., 1T and 2T. With all the parameters fixed for the material, the load-CMOD response is predicted for all the three specimen sizes. The results are shown in Fig. 16 along with the experimental data. It can be observed that the nonlocal model is not only able to predict the response with different mesh sizes as shown in Fig. 15, it is also able to predict the geometric effect of specimen size on the load-CMOD response very accurately. Hence, the parameter transferability issue is also valid for the nonlocal formulation.
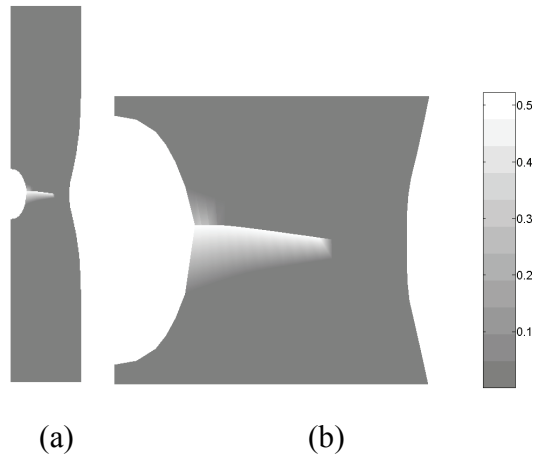
Figure 13: (a) Prediction of crack path in the flat tensile specimens using local damage model, (b) enlarged view near the central region
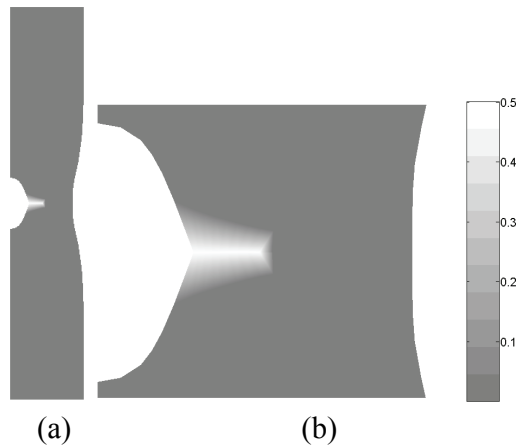

Figure 14: (a) Prediction of crack path in the flat tensile specimens using nonlocal damage model, (b) enlarged view near the central region
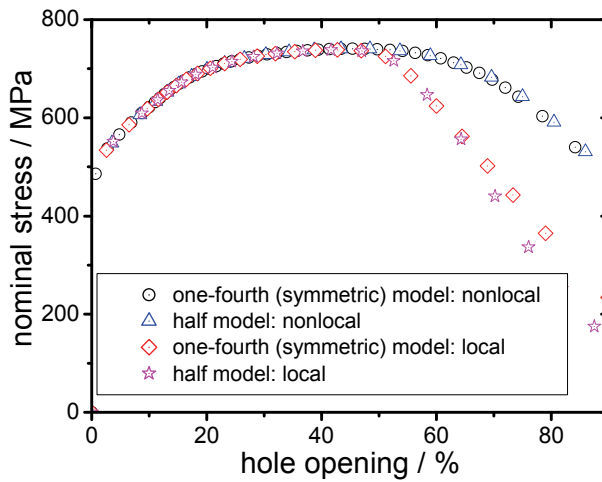
Figure 15: Nominal stress vs %age hole opening behaviour of the flat tensile specimen with hole at centre (effect of symmetric modeling with local and nonlocal models)
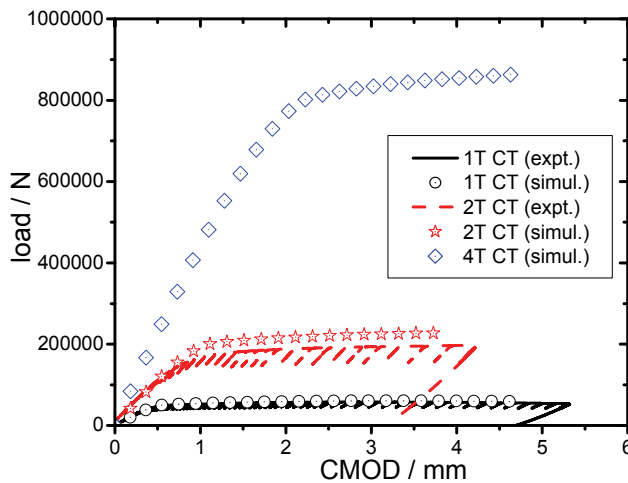

Figure 16: Prediction of geometry effect (effect of specimen size) on load-CMOD response of CT specimen with the help of nonlocal model

The next example is regarding the prediction of fracture toughness variation with temperature in the DBTT region. The results presented are for the pressure vessel steel DIN 22NiMoCr3-7. The standard 1T CT specimen has been analysed with the new nonlocal formulation at different temperatures and the results are shown in Fig. 17.
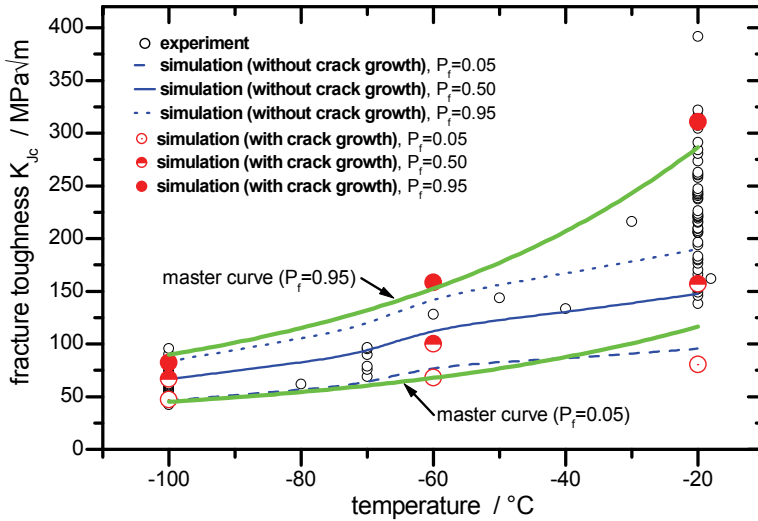

Figure 17: Comparison of predicted fracture toughness variation in the DBTT regime for the standard CT specimen with experiment and master curve

It is now very clear that the nonlocal model is able to predict the fracture toughness scatter and mean values across the whole DBTT temperature range very accurately. This is due to the ability to use very fine mesh and predict the micron-scale stable crack growth before unstable fracture by the process of cleavage. The results are also compared with the predictions of the master curve which is an empirical equation. However, one needs to know the value of transition temperature T_0 in order to plot such a curve. This value of transition temperature in the master curve is also dependent upon the specimen type, geometry and loading conditions and it is also different in case of actual components with varying geometry, loading and crack configurations. It is not possible to know the value of T_0 in advance for the component geometry of interest, which is a major limitation of this empirical master curve approach. However, a conservative estimate of T_0 is usually used for safety

evaluation which may not be optimum. These nonlocal models are based on physically and microscopically motivated damage processes and as these are based on material constitutive formulations; they do not have such limitations as discussed above. Hence, the model should be able to predict the fracture toughness variation across the DBTT regime for different specimen types and loading conditions which will be demonstrated in the following paragraphs.

Fig. 18 shows the results of the nonlocal model for the scatter in fracture toughness values in the testing of a 2T compact tension specimen in the DBTT regime.
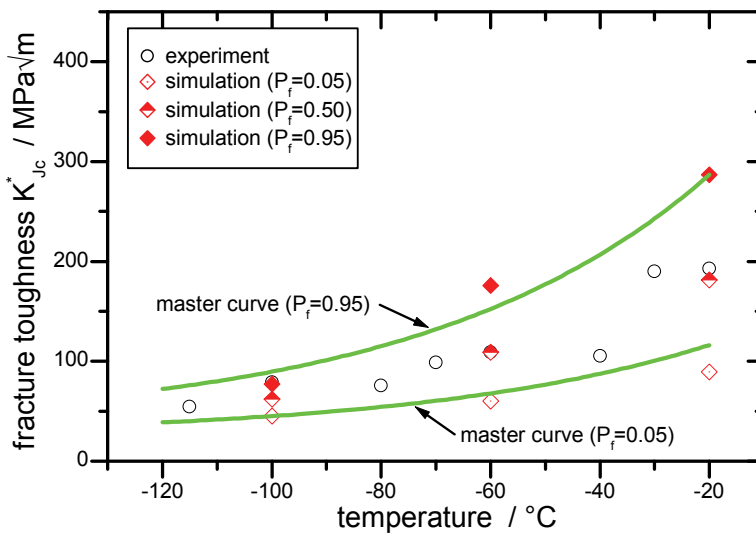

Figure 18: Comparison of simulated (with nonlocal damage damage) scatter of fracture toughness with experiment in the transition temperature region for a 2T CT specimen. * stands for the value of K_{JC} which is not corrected for specimen size effect

The predictions are very close to those of experiment. Another specimen type (i.e., a standard single-edged cracked specimen loaded in three-point bending as shown in Fig. 19) is considered here for the demonstration.

The results of the local model are shown in Fig. 19, whereas the results of the nonlocal model are presented in Fig. 20. It is again observed that the nonlocal model is able to predict the scatter in fracture toughness very accurately irrespective of specimen type and geometry. The local damage models are clearly inadequate for this purpose of safety analysis due to their inability to handle varying mesh sizes.
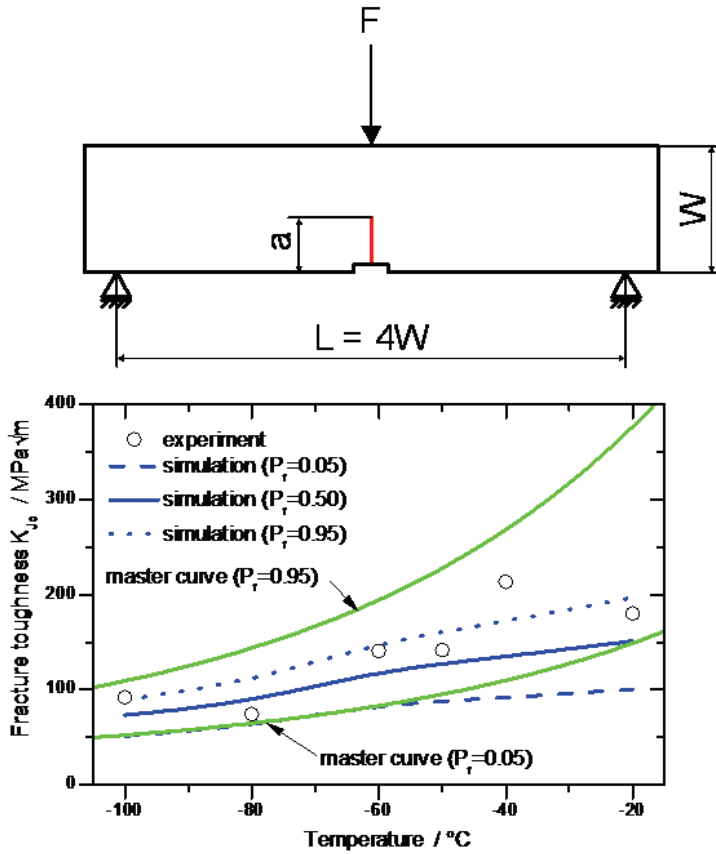
Figure 19: Inability of elasto-plastic and the local damage models to predict fracture toughness transition curve in the DBTT regime for a standard 1T three point bend specimen

7 Conclusions

In this work, a scheme for nonlocal regularization of the damage mechanics constitutive equations was presented. It was demonstrated that such a scheme is necessary in order to carry the safety analysis task in situations involving simulation of sub-millimetre crack growths, small specimens, steep stress gradients etc. Though the local damage models have been used effectively to predict the ductile crack growth behaviour of different types of specimens and components, the issue of using a constant mesh size limits its applications in many other situations. With this
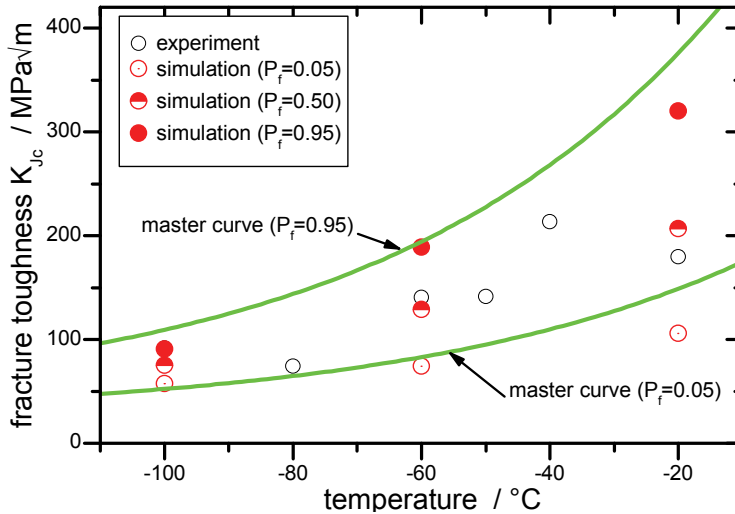
Figure 20: Comparison of predicted fracture toughness variation in the DBTT regime for the standard 1T three point bend specimen with experiment and master curve

new model, the analysts will have an effective tool for efficient and reliable safety analysis. The future task will be the extension of these models for simulation of response in other loading conditions such as low-cycle fatigue and creep.

References

Aifantis, E. C. (2001): Gradient plasticity, *Handbook of Materials Behavior Models, Ed. J. Lemaitre. Academic Press, New York*, pp. 281-297.

ASTM-E 1921-05 (2005): Standard test method for determination of reference temperature for ferritic steels in the transition range, *American Society for Testing and Materials, 1921-05.*

Bazant, Z. P.; Belytschko, T. (1987): Proceedings of the 2nd international confer-

ence on constitutive laws for engineering materials: *Theory and Applications. Eds. C. S. Desai and R. H. Gallagher. Elsevier, New York.*

Beremin, F. M. (1983): A local criterion for cleavage fracture of a nuclear pressure vessel steel, *Metall. Trans. A, 14A,* pp. 2277-2287.

Eberle, A.; Klingbeil; Schicker, J. (2000): The calculation of dynamic J_R-curves from the finite element analysis of a Charpy test using a rate-dependent damage model, *Nuclear Engineering and Design*, vol. 198, no. 1-2, pp. 75-87.

Eisele, U. (2006): Critical examination of the master curve approach regarding application in German nuclear power plants, Final Report, Reactor Safety Research -Project No. 1501 240, *Materialprüfungsanstalt Universität Stuttgart, Germany.*

Gurson, A. L. (1977): Continuum theory of ductile rupture by void nucleation and growth: Part-I: Yield criteria and flow rules for porous ductile media, *Transactions of ASME Journal Engineering Materials and Technology* vol. 99, pp. 2-15.

Geers, M. G. D.; de Borst, R.; Brekelmans, W. A. M.; Peerlings, R. H. J. (1998): Strain-based transient-gradient damage model for failure analyses, *Computer Methods in Applied Mechanics and Engineering* vol. 60, pp. 133–153.

Gao, X.; Ruriggieri, C.; Dodds, R. H. (1998): Calibration of Weibull stress parameters using fracture toughness data, *Int. J. Fract.,* vol. 92, pp. 175-200.

Gao, X.; Dodds, R. H.; Tregoning, R. L.; Joyce, J. A.; Link. R. E. (1999): A Weibull stress model to predict cleavage fracture in plates containing surface cracks, *Fatigue Fract. Eng. Mater. Struct.,* vol. 22, pp. 481-493.

Gao, X.; Dodds, R. H.; Tregoning, R. L.; Joyce. J. A. (2001): Weibull stress model for cleavage fracture under high-rate loading, *Fatigue Fract. Eng. Mater. Struct.,* vol. 24, pp. 551-564.

Gao, X.; Dodds, R. H. (2005): Loading rate effects on parameters of the Weibull stress model for ferritic steels, *Eng. Fract. Mech.* vol. 72, pp. 2416-2425.

Kussmaul, K.; Eisele, U.; Seidenfuss, M. (1995): On the applicability of local approach models for the determination of the failure behaviour of steels with different toughness, *In Fatigue and fracture mechanics in pressure vessel and piping (Eds Mehta et al.)*, vol. 304, pp. 17–25 (ASME, NewYork).

Needleman, A.; Tvergaard, V. (1984): An analysis of ductile rupture in notched bars, *Journal of the Mechanics and Physics of Solids* vol. 32, pp. 461-490.

Pitard Bouet, J. M.; Seidenfuss, M.; Bethmont, M.; Kussmaul, K. (1999): Experimental investigations on the shallow crack effect on the 10 MnMoNi 5 5 steel and computational analysis in the upper shelf by means of the global and local approaches, *Nuclear Engineering and Design* vol. 190, pp. 171-190.

Pavankumar, T.V.; Samal, M. K.; Chattopadhyay, J.; Dutta, B. K.; Kushwaha,

H. S.; Roos, E.; Seidenfuss, M. (2005): Transferability of fracture parameters from specimens to component level, *International Journal of Pressure Vessels and Pipings* vol. 82, no. 5, pp. 386-399.

Peerlings, R. H. J.; De Borst, R.; Brekelmans, W. A. M.; Geers, M. G. D. (2002): Localisation issues in local and nonlocal continuum approaches to fracture, *European Journal of Mechanics A-Solids* vol. 21, pp. 175–189.

Petti, J.; Dodds, R. H. (2005): Calibration of the Weibull stress scale parameter, using the master curve, *Eng. Fract. Mech.,* vol. 72, pp. 91-120.

Rice, J. R.; Tracey, D. M. (1969): On the Ductile enlargement of voids in triaxial stress fields, *Journal of the Mechanics and Physics of Solids* 17, pp. 201-217.

Rousselier, G. (1987): Ductile fracture models and their potential in local approach of fracture, *Nuclear Engineering and Design* vol. 105, pp. 97-111.

Reusch, F.; Svendsen, B.; Klingbeil, D. (2003): A non-local extension of Gurson-based ductile damage modelling, *Computational Materials Science* vol. 26, pp. 219-229.

Reusch, F.; Svendsen, B.; Klingbeil, D. (2003): Local and non-local Gurson-based ductile damage and failure modelling at large deformation, *European Journal of Mechanics A/Solids* vol. 22, pp. 779–792.

Rettenmeier, P. (2009): Implementierung eines nichtlokalen Schädigungsmodells in das Finite Elemente Programm ANSYS, *Studienarbeit, Institut für Materialprüfung, Werkstoffkunde und Festigkeitslehre (IMWF) Universität Stuttgart, Germany.*

Roos, E.; Schuler, X.; Silcher, H.; Seebich, H.P; Eisele, U. (2005): Classification of the Mastercurve Concept within the Framework of Safety Assessments Based on Mechanics of Materials, *Proceedings of the 18th International Conference on Structural Mechanics in Reactor Technology (SMiRT 18), Paper G01-4, Beijing, China.*

Svendsen, B. (1999): On the thermodynamic of thermoelastic materials with additional scalar degrees of freedom, *Continuum Mechanics and Thermodynamics* vol. 4, pp. 247-262.

Samal, M. K.; Seidenfuss, M.; Roos, E.; Dutta, B. K.; Kushwaha, H. S. (2008): Finite element formulation of a new nonlocal damage model, *Finite Elements in Analysis and Design* vol. 44, no. 6-7, pp. 358-371.

Samal, M. K.; Seidenfuß, M.; Roos, E.; Dutta, B. K.; Kushwaha, H. S. (2007): Development of a nonlocal damage mechanics model 33, *MPA Seminar, Stuttgart, Germany.*

Seidenfuss, M.; Roos, E. (2004): LISSAC-size and geometry effects on the failure behaviour of notched specimens, 30th *MPA Seminar, MPA, University of Stuttgart,*

Germany.

Seebich, H. P. (2007): Doctoral dissertation, *Institut für Materialprüfung Werkstoffkunde und Festigkeitslehre, Universität Stuttgart, Germany.*

Tvergaard, V.; Needleman, A. (1984): Analysis of cup-cone fracture in a round tensile bar, *Acta Metallurgica* vol. 32 no. 1, pp. 157-169.

Wallin, K. (1999): Master curve method: a new concept for brittle fracture, *Int. J. Mater. Product. Technol.*, vol. 14, pp. 342-354.

Wallin, K. (1991): Fracture toughness transition curve shape for ferritic structural steels. In: Fracture of Engineering Materials and Structures (Edited by S.T. Keoh and K.H. Lee), *Elsevier Applied Science*, pp. 83-88.